Journal of Engineering Mathematics manuscript No.
(will be inserted by the editor)

Wavemaker theories for acoustic-gravity waves over a finite depth

Miao Tian · **Usama Kadri**

Received: date / Accepted: date

Abstract Acoustic-gravity waves (hereafter AGWs) in ocean have received much interest recently, mainly with respect to early detection of tsunamis as they travel at near the speed of sound in water which makes them ideal candidates for early detection of tsunamis. While the generation mechanisms of AGWs have been studied from the perspective of vertical oscillations of seafloor and triad wave-wave interaction, in the current study we are interested in their generation by wave-structure interaction with possible implication to the energy sector. Here, we develop two wavemaker theories to analyse different wave modes generated by impermeable (the classic Havelock's theory) and porous (porous wavemaker theory) plates in weakly compressible fluids. Slight modification has been made to the porous theory so that, unlike the previous theory, the new solution depends on the geometry of the plate. The expressions for three different types of plates (piston, flap, delta-function) are introduced. Analytical solutions are also derived for the potential amplitude of the gravity, acoustic-

Miao Tian

1. Department of Physical Oceanography, Woods Hole Oceanographic Institute, Woods Hole, MA 02543, USA.

2. The Hatter Department of Marine Technologies, University of Haifa, Haifa 3498838, Israel.

3. INTERA Incorporated, Gainesville, FL 32606, USA.

E-mail: mtian@whoi.edu

Usama Kadri

1. The Hatter Department of Marine Technologies, University of Haifa, Haifa 3498838, Israel.

2. School of Mathematics, Cardiff University, Cardiff, CF24 4AG, UK.

3. Department of Mathematics, Massachusetts Institute of Technology, Cambridge, MA 02139, USA.

E-mail: ukadri@mit.edu

gravity, evanescent waves, as well as the surface elevation, velocity distribution, and pressure for AGWs. Both theories reduce to previous results for incompressible flow when the compressibility is neglected. We also show numerical examples for AGWs generated in a wave flume as well as in deep ocean. Our current study sets the theoretical background towards remote sensing by AGWs, for optimised deep ocean wave-power harnessing, among others.

Keywords wavemaker · Havelock's · porous · acoustic-gravity waves

1 Introduction

Wavemaker theory has received increasing attention not only because its feasibility on generating waves in laboratory experiments, but also due to its application in design of wave-energy harvesting devices [1]. The classic problem of surface waves generated by a wavemaker in infinitely deep ocean was investigated by Havelock, as in Ref. [2], and later extended to the case of finite water depth [3]. The wavemaker was treated as a vertical impermeable plate which oscillates horizontally and periodically with a small displacement, and the fluid was assumed incompressible. In all these formulations the wave motion was governed by linear wave theory. Extensions to a directional wavemaker problem with slowly-varying depth can be found in [4].

The impermeability of the plate is unrealistic for a plate in a wave flume, not to mention a landslide in deep ocean. Madsen [5] examined the influence of leakage around the wavemaker on the wave amplitude and concluded that the porous effect can largely reduce the wave amplitude. Therefore it would be more appropriate to take porosity effects into account for many applications.

Here, we study the effect of water compressibility and the generation of acoustic-gravity waves (AGWs) by water-structure interactions. AGWs have received much interest recently, as they travel at the speed of sound in water which makes them, among others, ideal precursors of tsunami by employing bottom-pressure recordings [6, 7]. AGWs can interact with continental shelves [8], ice-sheets [9], and might be responsible for deep-ocean water transportation and circulation [10]. In contrast to the decaying vertical structure of gravity-wave modes, the wave amplitudes of AGWs exhibit sinusoidal variation in the vertical direction. Therefore wave-energy harnessing devices that are placed in deep water (where the decaying

gravity wave modes vanish) can potentially make use of AGWs, whereby the induced measurable pressure signature may reach a maximum at the seabed. While harnessing energy of AGWs might become possible in the future, e.g. based on a triad interaction mechanism similar to that proposed by Refs. [11] or [12], a more immediate application is the detection of sea-state in wave harnessing farms. Here, we show that AGWs radiate by the harnessing devices, or namely wavemakers, carrying information on their source at the speed of sound in water. To this end, while the generation mechanisms of AGWs have been studied from the perspective of vertical oscillations of seafloor [13,7,14] and triad wave-wave interaction [15,16,11,12], here we are particularly interested in their generation by horizontally-moving wavemakers.

In this paper, we develop Havelock's and porous wavemaker theories for weakly compressible fluids. The paper is organised as follows: the problem is formulated with the governing equations and boundary conditions in section 2. The general solution is provided in Section 3, followed by the Havelock's and porous-wavemaker solutions in Section 4. Section 5 presents examples for three types of wavemakers placed in a wave flume as well as in deep ocean. The work is summarised in Section 6.

2 Governing equations

We take x and z the horizontal and vertical coordinates respectively, and consider a wavemaker with its plate initially located at $x = 0$. The wavemaker oscillates horizontally along the x-axis with a displacement s_0 given by

$$s_0(x,z,t) = d(z)\exp(-\mathrm{i}\omega t), \quad d \ll h, \tag{1}$$

where ω is the radian frequency, $d(z)$ is the maximum amplitude of oscillation, assumed to be much smaller than the undisturbed fluid depth h, and t is the time. The horizontal velocity and acceleration of the wavemaker are

$$u_0 = -\mathrm{i}\omega d\exp(-\mathrm{i}\omega t), \quad a_0 = -\omega^2 d\exp(-\mathrm{i}\omega t). \tag{2}$$

The equation that governs the irrotational motions of acoustic-gravity waves throughout the entire water column is

$$\Phi_{tt} = c^2(\Phi_{xx} + \Phi_{zz}), \quad -h < z < \eta, \tag{3}$$

where Φ is the velocity potential, and c is the speed of sound in water. The linearized kinematic and dynamic conditions at the free surface are

$$\Phi_z = \eta_t, \quad z = \eta, \tag{4}$$

$$\Phi_t + g\eta = 0, \quad z = \eta, \tag{5}$$

where η is the free surface elevation. Expanding (4) and (5) at $z = 0$ and eliminating η yield the approximated surface boundary condition as shown in Ref. [17]

$$\Phi_{tt} + g\Phi_z = 0, \quad z = 0. \tag{6}$$

Finally the kinematic bottom boundary condition for a flat bottom is given by

$$\Phi_z = 0, \quad z = -h, \tag{7}$$

which indicates that the vertical velocity of the fluid must be zero at the bottom.

Equations (3), (6), and (7) formulate the linear problem of water wave propagation over a finite depth in a weakly compressible fluid. Appropriate along-channel boundary conditions, depending on the wavemaker type, are included to define the problem completely.

For the classic Havelock's wave-maker theory [2, 18, 3], the boundary condition is

$$\Phi_x = u_0, \quad x = 0. \tag{8}$$

Here, u_0 is the horizontal velocity of the stroke motion.

For a porous-wavemaker problem, the boundary condition at the wavemaker is given by Ref. [19]. The hydrodynamic pressure $p(x,z,t)$ is associated with the velocity potential Φ via the linearised Bernoulli equation as

$$p = -\rho\Phi_t \tag{9}$$

in which ρ is the water density.

The pressure on the positive and negative sides of the wavemaker are related as

$$p(0,z,t) = p^+(z,t) = -p^-(z,t). \tag{10}$$

The normal velocity towards the porous plate is equal to the velocity of the stroke motion u_0, which is linearly proportional to the pressure difference between the two sides of the wavemaker [20], so that

$$u_0(z,t) = \frac{2b}{\mu} p(0,z,t). \tag{11}$$

Here, μ is the dynamic viscosity, and b is the coefficient which represents the width of the plate and has the dimension of length.

3 General Solution

Because of the periodic motion of the wavemaker, Φ, η, and p are assumed to be periodic functions in t with a time factor $\exp(-\mathrm{i}\omega t)$, i.e.

$$\Phi = \phi(x,z)\exp(-\mathrm{i}\omega t), \quad \eta = a(x)\exp(-\mathrm{i}\omega t), \quad p = p(x,z)\exp(-\mathrm{i}\omega t). \tag{12}$$

Using (12), equation (3) reduces to the Helmholtz equation

$$\phi_{xx} + \phi_{zz} + k_c^2\phi = 0, \quad k_c = \omega/c, \tag{13}$$

where k_c is a compressibility coefficient. Similarly, substiting equation (12) into equations (6) and (7) yields the boundary conditions in terms of ϕ,

$$-\omega^2\phi + g\phi_z = 0, \quad z = 0; \tag{14}$$

$$\phi_z = 0, \quad z = -h. \tag{15}$$

Following similar steps as in Refs. [7] and [14] the solution of equations (13)-(15) is obtained,

$$\begin{aligned}\phi &= A_0\exp(\mathrm{i}k_0x)\cosh(\lambda_0(z+h)) \\ &+ \sum_{n=1}^{N} A_n\exp(\mathrm{i}k_nx)\cos(\lambda_n(z+h)) \\ &+ \sum_{n=N+1}^{\infty} B_n\exp(-\kappa_nx)\cos(\lambda_n(z+h)),\end{aligned} \tag{16}$$

where λ_0 and λ_n are real and positive solutions of the following dispersion relationships

$$\omega^2 = g\lambda_0\tanh(\lambda_0h); \tag{17}$$

$$\omega^2 = -g\lambda_n\tan(\lambda_nh), \quad n = 1,2,3,\ldots, \tag{18}$$

where λ_n is the n-th eigenvalue and n is the mode number. With specified ω and h, equation (17) has one real solution for λ_0; while equation (18) involves infinitely-many different eigenvalues.

The parameters k_0, k_n, κ_n are all real and positive, given by

$$k_0 = \sqrt{k_c^2 + \lambda_0^2}, \tag{19}$$

$$k_n = \sqrt{k_c^2 - \lambda_n^2}, \quad n = 1,2,...,N; \quad k_c > \lambda_N, \tag{20}$$

$$\kappa_n = \sqrt{\lambda_n^2 - k_c^2}, \quad n = N+1, \ldots; \quad k_c < \lambda_{N+1}, \tag{21}$$

where

$$N = \left\lfloor \frac{\omega h}{\pi c} + \frac{1}{2} \right\rfloor \tag{22}$$

represents the number of existing AGW modes, and the brackets is the floor function (nearest integer from below), as in Ref. [8]. The three terms on the right-hand-side of equation (16) represent the gravity, acoustic-gravity, and evanescent modes, respectively.

4 Wavemaker problem

4.1 Solution for Havelock's wavemaker

Since $\cosh(\lambda_0(z+h))$ and $\cos(\lambda_n(z+h))$ in equation (16) are the eigenfunctions of the boundary value problem in z, they are orthogonal over the interval from $z=0$ to $z=-h$ based on the Sturm-Liouville theory. Therefore, we substitute equations (12) and (16) into equation (8), multiply by $\cosh(\lambda_0(z+h))$ and $\cos(\lambda_n(z+h))$ and integrate over the water column from $z=-h$ to $z=0$ so that A_0, A_n, B_n can be calculated as

$$A_0 = \frac{-2\omega}{h\sqrt{k_c^2+\lambda_0^2}\,(1+CQ_0^2)} \int_{-h}^{0} d\cosh(\lambda_0(z+h))\,\mathrm{d}z, \tag{23}$$

$$A_n = \frac{-2\omega}{h\sqrt{k_c^2-\lambda_n^2}\,(1-CQ_n^2)} \int_{-h}^{0} d\cos(\lambda_n(z+h))\,\mathrm{d}z, \tag{24}$$

$$B_n = \frac{2\mathrm{i}\omega}{h\sqrt{\lambda_n^2-k_c^2}\,(1-CQ_n^2)} \int_{-h}^{0} d\cos(\lambda_n(z+h))\,\mathrm{d}z, \tag{25}$$

where

$$Q_0 = \sinh\lambda_0 h, \quad Q_n = \sin\lambda_n h, \quad C = \frac{g}{\omega^2 h}. \tag{26}$$

In the incompressible case ($c \to \infty$), equations (23) and (25) reduce to the solutions for gravity and evanescence modes in [21] (equations (6.21) and (6.22)). The extra term A_n comes from the newly-generated AGW mode due to the compressibility of the fluid.

4.2 Solution for porous wavemaker

Following similar steps using (11) together with (9), (12), and (16) and the orthogonality of $\cosh(\lambda_0(z+h))$ and $\cos(\lambda_n(z+h))$, we can derive expressions of A_0, A_n, B_n for a porous wavemaker. Chwang [19] described a similar problem for incompressible flow and derived the solutions. Chwang's solution, however, indicates that the produced waves have the same amplitudes regardless to the geometry of the plate. In order to consider different plate types, we modify Chwang's method and derive an alternative solution in a similar form as the Havelock's [21]

$$A_0 = G_0 \frac{-2\omega}{h\sqrt{k_c^2+\lambda_0^2}\left(1+CQ_0^2\right)} \int_{-h}^{0} d\cosh(\lambda_0(z+h))\,\mathrm{d}z, \tag{27}$$

$$A_n = G_n \frac{-2\omega}{h\sqrt{k_c^2-\lambda_n^2}\,(1-CQ_n^2)} \int_{-h}^{0} d\cos(\lambda_n(z+h))\,\mathrm{d}z, \tag{28}$$

$$B_n = H_n \frac{2\mathrm{i}\omega}{h\sqrt{\lambda_n^2-k_c^2}\,(1-CQ_n^2)} \int_{-h}^{0} d\cos(\lambda_n(z+h))\,\mathrm{d}z, \tag{29}$$

where the porous factors are

$$\begin{aligned} G_0 = \frac{\mu\sqrt{k_c^2+\lambda_0^2}}{2\omega\rho b}, \quad G_n = \frac{\mu\sqrt{k_c^2-\lambda_n^2}}{2\omega\rho b}, \quad n = 1,2,\ldots N, \\ H_n = \frac{-\mathrm{i}\mu\sqrt{\lambda_n^2-k_c^2}}{2\omega\rho b} \quad n = N+1, N+2, \ldots. \end{aligned} \tag{30}$$

We focus on the porous factor G_n that is associated with AGW modes. As pointed out in [19], the reciprocal of G_n in equation (30) can be understood as a Reynolds number for the flow passing through the porous wavemaker, while G_n also measures the porosity. For example, $G_n = 0$ (or equivalently, $\mu = 0$) corresponding to a wavemaker that is completely permeable. Obviously, the expressions reduce to the Havelock's solution when the porous factors, G_0, G_n, H_n, are unity. Moreover, as λ_n increases with the mode number n, the porous factor G_n decreases for higher AGW modes, meaning that the porous media dissipates more energy from shorter waves (lower modes). Specifying values for the porous factor of the gravity mode G_0 (0.1, 0.2, 0.5, etc.), Chwang [19] presented the surface elevation of gravity waves produced by the wavemaker. In this study, the porous factor for the first AGW mode G_1 will be set to 0.5 for illustration purposes, while G_n $(n = 2,3,\ldots)$ can be determined accordingly.

The amplitudes of the surface elevation, horizontal velocity, and pressure at AGW mode n can also be given employing equations (5), (9), (12), (16)

$$a_n = \mathrm{i}\frac{\omega}{g}A_n \exp\left(\mathrm{i}\sqrt{k_c^2-\lambda_n^2}x\right)\cos\left(\lambda_n h\right); \tag{31}$$

$$u_n = \mathrm{i}\sqrt{k_c^2-\lambda_n^2}A_n \exp\left(\mathrm{i}\sqrt{k_c^2-\lambda_n^2}x\right)\cos\left(\lambda_n\left(z+h\right)\right); \tag{32}$$

$$p_n = \mathrm{i}\omega\rho A_n \exp\left(\mathrm{i}\sqrt{k_c^2-\lambda_n^2}x\right)\cos\left(\lambda_n\left(z+h\right)\right); \tag{33}$$

where A_n is defined in equation (28).

4.3 Different types of plates

We focus on the AGWs term in equations (24) and (28) and derive the explicit form based on different types of plates. Piston and flap motions [21] are commonly used for wave flumes in laboratory experiments, while a wavemaker of δ-function type is considered for deep ocean [18]. Therefore the function $d\left(z\right)$ that describes the piston motion in equation (1) has been assumed to be

$$d\left(z\right) = \begin{cases} D, & \text{piston plate;} \\ D\left(1+z/h\right), & \text{flap plate;} \\ D\delta\left(z+h_0\right), & \delta\text{-function plate.} \end{cases} \tag{34}$$

Here, D is the horizontal amplitude of the stroke motion. The δ-function type wavemaker is located at $z=-h_0$.

Substituting equation (34) into the Havelock's solution (24), the expression for the amplitude A_n of the velocity potential can be readily obtained in the form

$$A_n = \begin{cases} M_n \sin\left(\lambda_n h\right), & \text{piston plate;} \\ \dfrac{M_n}{\lambda_n h}\left[\lambda_n h\sin\left(\lambda_n h\right)+\cos\left(\lambda_n h\right)-1\right], & \text{flap plate;} \\ M_n\cos\left(\lambda_n\left(h-h_0\right)\right), & \delta\text{-function plate.} \end{cases} \tag{35}$$

in which

$$M_n = \frac{-2\omega D}{\lambda_n h\sqrt{k_c^2-\lambda_n^2}\left(1-CQ_n^2\right)}. \tag{36}$$

A comparison of the normalised velocity potential amplitude in equation (35) is given in Figure 1. For illustration, the δ-function in (34) is assumed to be located at the depth $z=-h_0=-h/2$. Apparently, a flap wavemaker produces the largest first-mode AGW for

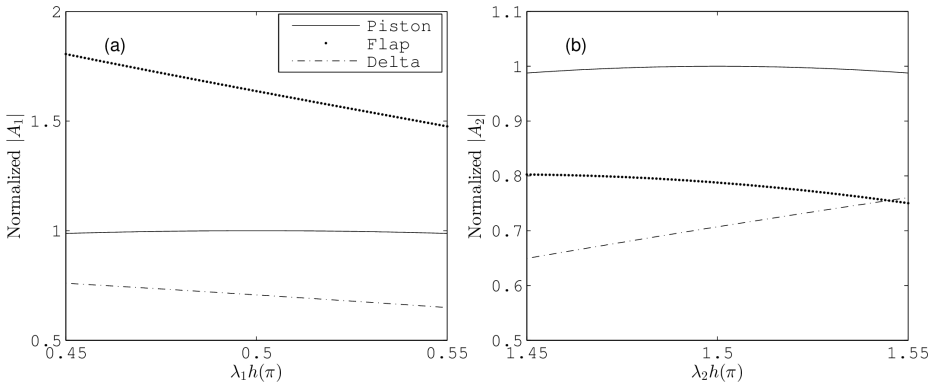

Fig. 1 normalised AGW velocity potential amplitudes $|A_1|$ (a) and $|A_2|$ (b) by a factor of M_n ($n = 1$ and 2, respectively) for three types of plate as a function of $\lambda_n h$, which is chosen to vary between $[0.45, 0.55]n\pi$. The δ-function type wavemaker is assumed to be located at $z = -h/2$ for illustration purposes. Solid: piston-type plate; dotted: flap-type plate; dashed: δ-function type plate.

the same plate-motion amplitude D. For a flap plate, equation (35) also indicates that the normalised AGW amplitudes are inversely proportional to $\lambda_n h$, therefore higher AGW modes must have smaller normalised amplitudes.

5 Examples

5.1 Acoustic-gravity waves in a wave flume

The number of existing AGW modes associated with specific frequency and depth are calculated by (22). This relation shows that more AGW modes can be generated at a higher frequency ω or impractically deep water. Therefore, generating AGWs in the laboratory is not an easy task. In order to obey AGW theory (with the absence of bottom elasticity, e.g. see Ref. [22] for the detailed analysis) and create AGWs in the laboratory experiments we need to operate at relatively very high frequencies. For example, there are three AGW modes corresponding to a 5 kHz wavemaker in a 0.5 m wave flume. Although working with a 5 kHz source introduces some real difficulties, we can still have feasible experiments with piezoelectric membranes to validate the proposed theory (an on-going research effort). Alternatively, one needs to carry out an experiment in the deep ocean, which is by no means easier to perform. Due to this conflicting choice of an appropriate experimental environ-

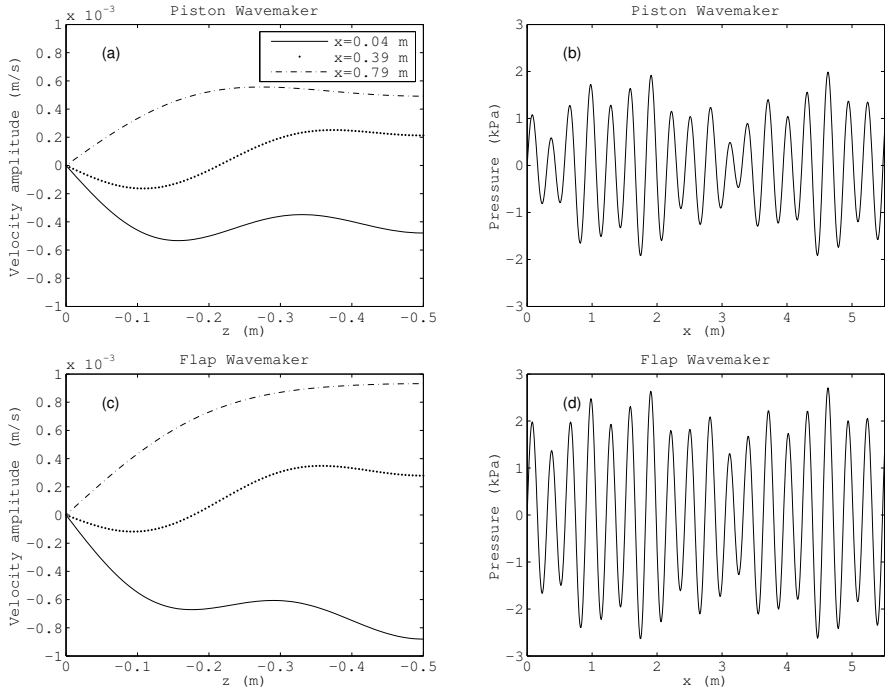

Fig. 2 Acoustic-gravity waves generated by a wavemaker in a wave flume for $f = 5$ kHz based on the Havelock's wavemaker theory; $L = 5.5$ m, $h = 0.5$ m, $b = 1$ m, $c = 1500$ m/s. The motion of the plate is limited by the constraint that, the horizontal movement ≤ 2.1 m, the horizontal velocity ≤ 3.8 m/s, horizontal acceleration ≤ 19.6 m/s^2 (parameters come from the unidirectional wavemaker in O.H. Hinsdale Wave Research Laboratory, Oregon State University). (a), (c) Vertical distribution of the velocity amplitude at $x = 0.04$ m, 0.39 m, and 0.79 m away from the wavemaker. (b), (d) Horizontal distribution of the pressure amplitude at the bottom of the flume. (a), (b) piston wavemaker; (c), (d) flap wavemaker.

ment, we dedicate this section and the following to the disparate wave flume and deep ocean systems, respectively.

Examples of AGWs generated in a wave flume by piston- and flap-type plates are shown in Figures 2 and 3 based on Havelock's and porous wavemaker theories, respectively. Notice that the stroke motion is not only limited by its maximum stroke distance, but also the maximum velocity and acceleration. Here, we assume that the wavemaker has the same constraints as the unidirectional wavemaker of the O.H. Hinsdale Wave Research Laboratory in Oregon State University (for example the laboratory experiment presented in Ref. [23]); a simple calculation using equations (2) shows that the stroke amplitude of a wavemaker with $f = 5$ kHz is in the order of 10^{-8} m, which requires a very careful experiment.

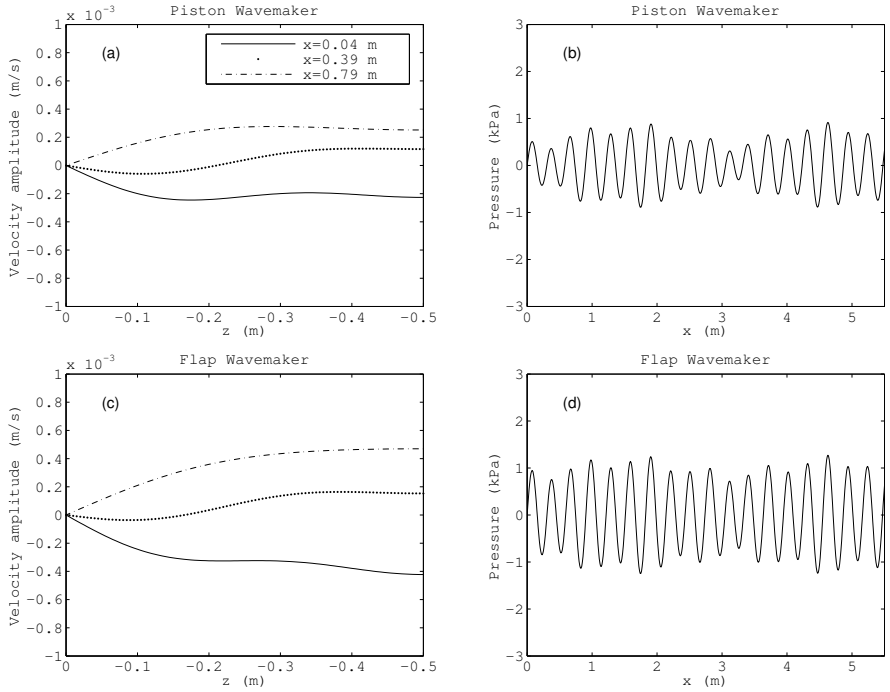

Fig. 3 Acoustic-gravity waves generated by a wavemaker in a wave flume for $f = 5$ kHz based on the porous wavemaker theory; $L = 5.5$ m, $h = 0.5$ m, $b = 1$ m, $c = 1500$ m/s. The motion of the plate is limited by the constraint that, the horizontal movement ≤ 2.1 m, the horizontal velocity ≤ 3.8 m/s, horizontal acceleration ≤ 19.6 m/s^2 (parameters come from the unidirectional wavemaker in O.H. Hinsdale Wave Research Laboratory, Oregon State University). (a), (c) Vertical distribution of the velocity amplitude at $x = 0.04$ m, 0.39 m, and 0.79 m away from the wavemaker. (b), (d) Horizontal distribution of the pressure amplitude at the bottom of the flume. (a), (b) piston wavemaker; (c), (d) flap wavemaker.

It is difficult to measure AGW surface elevations directly due to their small amplitudes (not shown in the figure), whereas the horizontal velocity component which is in the order of 10^{-3} m/s (Figure 2 (a) and (c)), is detectable using a particle image velocimetry (PIV) system. It is also worth mentioning that, unlike gravity waves, the AGW velocity amplitude oscillates vertically and leaves a distinct pressure signature throughout the entire water column, and mainly at the bottom.

The time series of the pressure at the bottom (Figure 2 (b) and (d)) behaves in a similar way to the surface elevation, although measurable by a wired pressure sensor. Therefore, in spite of the small amplitude of their surface elevation, AGWs are expected to be detectable on bottom-pressure records or PIV velocity measurement in a laboratory study. On the other

hand the flap wavemaker is able to produce larger waves compared to the piston wavemaker as shown in Figure 2 (c) and (d). Figure 3 presents AGW-induced pressure and velocities produced by porous wavemakers. Due to the porosity effect, the velocity and pressure amplitudes are generally smaller than those of the Havelock's theory.

5.2 Acoustic-gravity waves in deep ocean

We treat the problem of a wavemaker plate in deep ocean as a point source in deep water (similar to the ocean acoustics problem in Ref. [24]) , and consider it as a δ-function. An example of a δ-function wavemaker located at $z = -12.5$ m in deep ocean with $f = 1$ Hz and $h = 4000$ m is presented in Figure 4 for both Havelock's and porous wavemaker theories. The AGWs produced by an impermeable wavemaker ($G = 0$) have larger amplitudes (Figure 4 (a) and (b)), whereas the wave amplitude decreases as the wavemaker becomes porous ($G \neq 0$). The surface elevation increases to 10^{-3} m (not shown) compared to those in the laboratory example, although still hard to be distinguished from that of surface gravity waves. The velocity amplitudes are almost zero at the surface; they reach a maximum at about $z = 500$ m, and oscillate across the water column in the z-direction. Although AGWs have frequencies similar to that of the gravity mode, their distributions are periodic throughout the water column (i.e. do not decay with depth). Therefore, they can be distinguished from the decaying gravity waves. The order of magnitude of the velocity reaches 10^{-2} m/s, which is measurable by standard instruments such as the ADCP (Acoustic Doppler Current Profiler), PCADP (Pulse-coherent Acoustic Doppler Profiler). It is thus suggested to employ pressure sensors at the seabed, or deep below the free surface, where surface-wave signatures are negligible. The AGW signal, however, is in the order of 10 kPa, which is easy to measure (e.g., the MODE experiment that measures the pressure fluctuation on the deep-sea floor by Ref. [25]). This simple example shows that AGWs may be responsible for the low-frequency oceanic noise on the seabed [26].

6 Conclusion

Without overlooking the slight compressibility of water, as is usually assumed, we present Havelock's and porous wavemaker theories to analyse different modes of water waves following Refs. [21] and [19], with a focus on AGW modes. These theories may have important

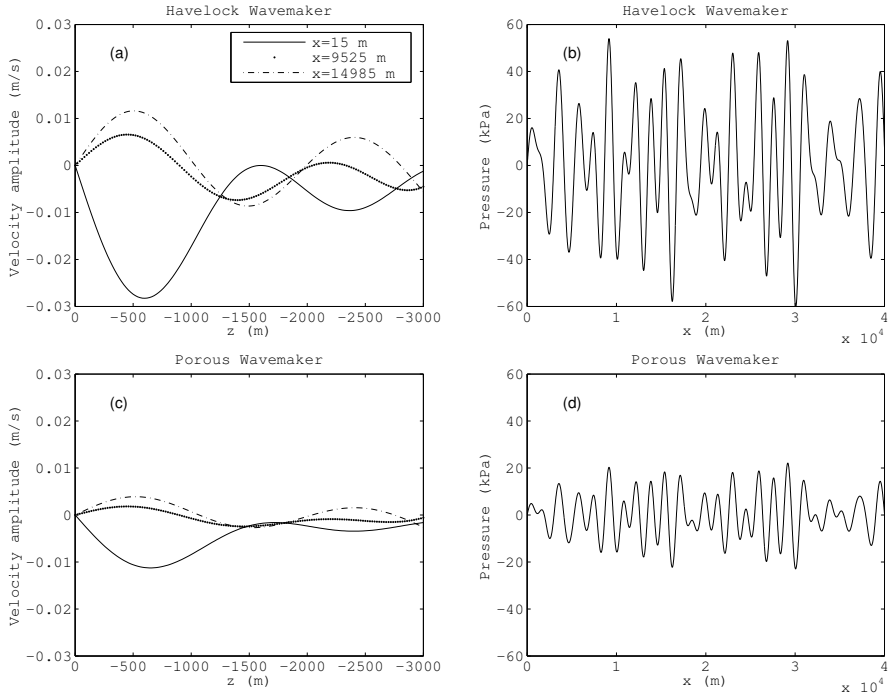

Fig. 4 Acoustic-gravity waves generated by a δ-function wavemaker in the ocean placed at $z = -12.5$ m for $f = 1$ Hz. The ocean is $h = 4000$ m deep and the speed of sound is $c = 1500$ m/s. (a), (c) Vertical distribution of the velocity amplitude at $x = 15$ m, 9525 m, and 14985 m away from the wavemaker. (b), (d) Horizontal distribution of the pressure amplitude at the bottom of the flume. (a), (b) Havelock's wavemaker theory; (c), (d) porous wavemaker theory.

implications in the study of surface waves in flume experiment [18] or tsunamis caused by landslides during earthquakes in deep ocean [8,7,14]. Moreover, the generation of AGWs can be attributed to wave-structure interaction [18], therefore another implication is where the efficiency of wave-energy harnessing devices is of interest, with the wavemaker being subjected to some form of wave energy converter, e.g., a flap gate [27]. Another and probably a more immediate implication is the remote detection of the wavy sea-state which can help tuning the surface wave energy converters for maximum efficiency. These are left for future studies, and we hope this work will motivate scientists and engineers to look into these important implications.

Both Havelock's and porous wavemaker solutions reduce to previous theories [19,21] for incompressible flow when the compressibility coefficient k_c in equation (13) tends to zero. The solutions for three types of plates as well as the spatial distribution of the AGW

components are presented. For the same horizontal plate displacements, a flap wavemaker is capable of making lager waves than piston and δ-function-type wavemakers. The spatial distribution of the amplitude of the surface elevation, horizontal velocity, and bottom pressure due to both theories shows that the porous wavemaker generally results in smaller waves than those produced by Havelock's theory due to the porosity factor G_n in equation (30). The calculations reveal that the surface elevation of AGWs in the current lab experimental settings is in the order of 10^{-9} m, and can reach 10^{-3} m in deep ocean. Consequently, surface elevation of AGWs is hard to measure; while velocity amplitude suggests that AGWs can be detected by a particle image velocimetry (PIV) system in the laboratory experiment. Finally, the pressure distributions show that AGW signals are significantly large at the bottom of a wave flume and deep ocean, to be captured by a standard pressure sensor. This study motivates further laboratory studies and field measurements on deep ocean as it predicts the characteristics of the generated waves, and provides insights on how to carry out direct measurements. It also sheds some light on the development of tsunami early-detection systems from the perspective of describing AGWs near the epicentre during earthquakes. Finally, the porous wavemaker theory can potentially contribute to the study of deep-ocean energy-harvest devices where the porous plates can be treated as an energy absorber.

Acknowledgements The first author acknowledges the Postdoctoral Scholar Program at the University of Haifa in collaboration with Woods Hole Oceanographic Institution.

References

1. Mei C.C., Hydrodynamic principles of wave power extraction, Phil. Trans. R. Soc. A 370 , 208-234 doi:10.1098/rsta.2011.0178, 2012.
2. Havelock T., Forced surface-waves on water, The London, Edinburgh, and Dublin Philosophical Magazine and Journal of Science, 8(51), 569-576, 1929.
3. Ursell F., Dean R.G., Yu Y.S., Forced small-amplitude water waves: a comparison of theory and experiment, J . Fluid Mech., 7, 33-52, 1960.
4. Dalrymple R.A., Directional wavemaker theory with sidewall reflection, J. Hydraul. Res., 27:1, 23-34, 1989.
5. Madsen O.S., Waves generated by a piston-type wavemaker, In Proc. 12th Coastal Engng Conf., 589-607, ASCE, 1970.
6. Hendin G., Stiassnie M., Tsunami and acoustic-gravity waves in water of constant depth, Phys. Fluids, 25, 086103, 2013.

7. Stiassnie M., Tsunamis and acoustic-gravity waves from underwater earthquakes, J. Eng. Math., 67, 23-32, doi:10.1007/s10665-009-9323-x, 2010.
8. Kadri U., Stiassnie M., Acoustic-gravity waves interacting with the shelf break, J. Geophys. Res., 117(C3), C03035, 2012.
9. Kadri U., Generation of Hydroacoustic Waves by an Oscillating Ice Block in Arctic Zones, Advances in Acoustics and Vibration, 8076108, http://dx.doi.org/10.1155/2016/8076108, 2016.
10. Kadri U., Deep ocean water transport by acoustic-gravity waves, J. Geophys. Res.: Oceans, 119(11), 7925-7930, 2014.
11. Kadri U., Triad resonance between a surface gravity wave and two high frequency hydro-acoustic waves, Eur J Mech B-Fluid, 55, 1, 157-161, 2016.
12. Kadri U., Akylas T.R., On resonant triad interactions of acoustic-gravity waves, J. Fluid Mech., 788: R1(12 pages), doi:10.1017/jfm.2015.721, 2016.
13. Oliveira T.C.A. and Kadri U., Pressure field induced in the water column by acoustic-gravity waves generated from sea bottom motion. J. Geophys. Res. Oceans. Accepted Author Manuscript. doi:10.1002/2016JC011742, 2016.
14. Yamamoto T., Gravity waves and acoustic waves generated by sub-marine earthquakes, Soil Dyn. Earthquake Eng., 1, 75-82, 1982.
15. Kadri U., Stiassnie M., Generation of an acoustic-gravity wave by two gravity waves, and their subsequent mutual interaction, J. Fluid Mech., 735, R61-R69, 2013.
16. Kadri U., Wave motion in a heavy compressible fluid: Revisited, Eur J Mech B-Fluid, 49(A), 50-57, 2015.
17. Lamb, H., Hydrodynamics, Cambridge: at the University Press, 4th edition, 352, 1916
18. Stuhlmeier R., Stiassnie M., Adapting Havelock's wave-maker theorem to acoustic-gravity waves, IMA J. Appl. Math., accepted.
19. Chwang A.T., A porous-wavemaker theory, J. Fluid Mech., 132, 395-406, 1983.
20. Taylor G.I., Fluid flow in regions bounded by porous surfaces, Proc. R. Soc. Lond. A234, 45-75, 1956.
21. Dean R.G., Dalrymple R.A., Water Wave Mechanics for Engineers and Scie ntists, Advanced Series on Ocean Engineering, 2, 174, World Scientific, 176, 1991.
22. Eyov E., Klar A., Kadri U., and Stiassnie M., Progressive waves in a compressible ocean with elastic bottom, Wave Motion 50, 929-939. doi: 10.1016/j.wavemoti.2013.03.003, 2013.
23. Tian M., Sheremet A., Kaihatu J.M., Ma G-F, On the Shoaling of Solitary Waves in the Presence of Short Random Waves, J. Phys. Oceanogr., 45, 3, 792-806, 2015.
24. Jensen F.B., Kuperman W.A., Porter M.B., and Schmidt, H., Computational Ocean Acoustics, Modern Acoustics and Signal Processing, ISBN 978-1-4419-8678-8, Springer, 2011.
25. Brown W., Munk W., Snodgrass F., Mofjeld H., Zetler B., MODE bottom experiment, J. Phys. Oceanogr., 5, 75-85, 1975.
26. Ardhuin F., Lavanant T., Obrebski M., Marie L., Royer J.-Y., D'Eu J.-F., Howe B. M., Lukas R., Aucan J., A numerical model for ocean ultra-low frequency noise: wave-generated acoustic-gravity and Rayleigh modes., J. Acoust. Soc. Am., 134(4), 3242-59, 2013.
27. Sammarco P., Michele S., d'Errico M., Flap gate farm: From Venice lagoon defense to resonating wave energy production. Part 1: Natural modes, Appl. Ocean Res., 43, 206-213, 2013.